Research Article | Vol. 31, No. 11 / 22 May 2023 / Optics Express 18693
Optics EXPRESS

Ampere force fiber optic magnetic field sensor using a Fabry-Perot interferometer

PEIJING CHEN,[1,†] GUIQING HONG,[1,†] SHEN LIU,[1,2,3,*] JUNLAN ZHONG,[1,3] WEI DING,[2,3] JUNXIAN LUO,[1] WENQI YAN,[2,3] HANG XIAO,[1,2] AND YIPING WANG[1,2,3]

[1] *Shenzhen Key Laboratory of Photonic Devices and Sensing Systems for Internet of Things, Guangdong and Hong Kong Joint Research Centre for Optical Fibre Sensors, State Key Laboratory of Radio Frequency Heterogeneous Integration, Shenzhen University, Shenzhen 518060, China*
[2] *Shenzhen Key Laboratory of Ultrafast Laser Micro/Nano Manufacturing, Key Laboratory of Optoelectronic Devices and Systems of Ministry of Education/Guangdong Province, College of Physics and Optoelectronic Engineering, Shenzhen University, Shenzhen 518060, China*
[3] *Guangdong Laboratory of Artificial Intelligence and Digital Economy (SZ), Shenzhen 518107, China*
[†] These authors contributed equally to this work.
[*] *shenliu@szu.edu.cn*

Abstract: The paper presents a novel fiber-optic vector magnetic field sensor using a Fabry-Perot interferometer, which consists of an optical fiber end face and a graphene/Au membrane suspended on the ceramic ferrule end face. A pair of gold electrodes are fabricated on the ceramic ferrule by femtosecond laser to transmit electrical current to the membrane. Ampere force is generated when an electrical current flows through the membrane in a perpendicular magnetic field. The change in Ampere force causes a shift in the resonance wavelength in the spectrum. In the magnetic field intensity range of 0 ~ 180 mT and 0 ~ -180 mT, the as-fabricated sensor exhibits magnetic field sensitivity of 5.71 pm/mT and 8.07 pm/mT. The proposed sensor has great potential application in weak magnetic field measurements due to its compact structure, cost-effectiveness, ease to manufacture, and good sensing performance.

1. Introduction

Magnetic field sensors play a key role in many important fields, such as national defense, aerospace, medical diagnosis, etc [1–3]. Optical fiber-based magnetic field sensors have attracted considerable attention due to its strong electromagnetic interference resistance, low cost, compact size, etc. During the past decades, several types of optical fiber magnetic field sensors based on different sensing principles have been proposed and demonstrated, including the Faraday effect [4,5], magnetostrictive effect [6,7], magnetic force [8], magnetic fluid [9] and other mechanisms. Among them, Faraday effect-based schemes have been proved to be feasible because they can directly measure the magnetic field. However, due to the small magneto-optical Verdet constant of silicon dioxide fibers, the sensitivity of the sensor is quite low [10]. Therefore, optical fiber magnetic field sensors based on magnetic responsive materials have been extensively studied to expand the application of magnetic field sensor. Generally, optical fibers and magnetic sensitive materials are combined to achieve magnetic field sensing detection. For example, magnetic fluid (MF), a stable colloidal solution formed by encapsulating magnetic nanoparticles with surfactants [11], has been widely used as a magnetically sensitive material due to its magneto-optical properties that adjust the refractive index under a magnetic field [12]. Another important magnetically responsive material is the magnetostrictive material, which uses the magnetostrictive effect to transfer the strain generated under the magnetic field to the optical fiber to achieve the purpose of measuring the magnetic field [13]. However, the use of magnetic response materials introduces inherent magnetic saturation [14] and hysteresis effects [15], which

#491629 https://doi.org/10.1364/OE.491629
Journal © 2023 Received 27 Mar 2023; revised 26 Apr 2023; accepted 10 May 2023; published 19 May 2023

significantly reduce the measurement range and lead to measurement errors. Recently, a novel magnetic field sensor based on Ampere force was reported to avoid the limitations of magnetic saturation and hysteresis effects [16–18]. However, this is an indirect detection method, and the metal wire is always combined with the optical fiber device to transfer the ampere force or Lorentz force to the optical fiber device for magnetic field sensing. In addition, the assembly of metal wires and fiber optic equipment is also a technical challenge.

The combination of Fabry-Perot (F-P) structure and two-dimensional(2D) material films have been widely used in high-sensitivity force sensing. For example, in 2022, Liu et al. [19] proposed a fiber optic graphene nano-mechanical sensor with high resolution and photothermal sensitivity of approximately 6.44 kHz/μW. In 2016, Yu et al. [20] developed a high sensitivity F-P pressure sensor by transferring MoS_2 films onto the ceramic ferrule end faces, achieving sensitivity of 89.3 nm/Pa. Moreover, 2D material films can also be combined with functional materials for applications in other areas. In 2019, Ma et al. [21] combined optical fiber with suspended palladium and graphene composite films to propose a compact fiber optic hydrogen sensor with detection limit of ~ 20 ppm and response time of ~ 18 s. Therefore, F-P sensor based on the combination of 2D material and optical fiber has become a research hotspot attributed to the characteristics of thin and sensitivity.

In this letter, we propose and demonstrate a novel optical fiber vector magnetic field sensor based on Fabry-Perot interferometer (FPI) structure consisting of fiber end face and graphene/Au membrane suspended on the aperture over the aperture of ceramic end face. Particularly, a pair of electrodes is etched on the ceramic ferrule by femtosecond laser to transmit current. Such a vector magnetic field sensor exhibits sensitivities of approximately 5.71 and 8.07 pm/mT at positive and negative magnetic field directions when the current flowing is 70 mA in the experiment. Moreover, these sensitivities could potentially be improved by changing the electrical current.

2. Sensing principle and sample fabrication

Figure 1 illustrates the structure and schematic of magnetic field fiber-optic sensor, including a Fabry-Perot (F-P) cavity, a pair of gold electrodes, and a suspended graphene/Au membrane.

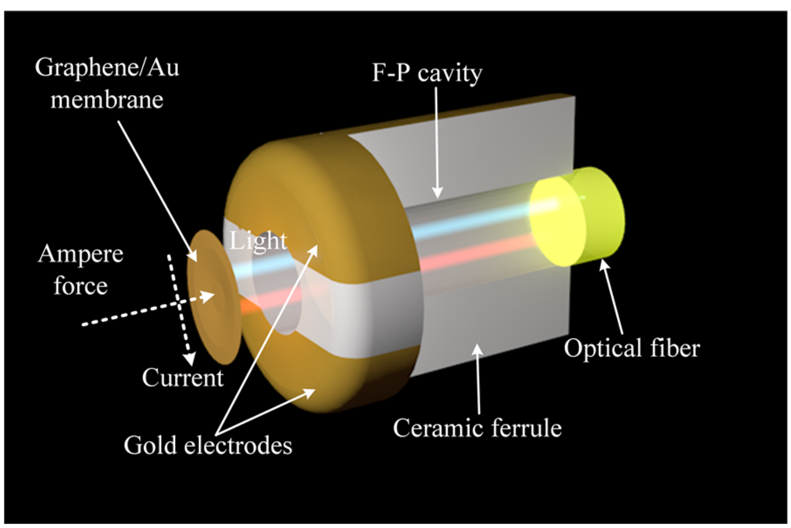

Fig. 1. Schematic of an FPI-based fiber optic magnetic field sensor.

The design and manufacture of magnetic field sensor include the following four steps. In the first fabrication step, the multilayer graphene is transferred onto the ceramic ferrule end

Optics EXPRESS

face using the wet transfer method [22]. In the second step, a gold membrane is coated on the ceramic ferrule end face by magnetron sputtering in order to make a pair of gold electrodes. During sputtering, the use of a rotating platform ensures uniform coating. The thickness of gold membrane can be controlled by adjusting sputtering time. In the third step, a pair of lapping films are used to scrape the Au membrane on the flank of the ceramic ferrule and left two parallel gap structures. Following that process, part of the Au layer on the ceramic ferrule end face is etched by a femtosecond laser to divide the gold film on the side into two parts. A ceramic ferrule with a pair of electrodes was prepared by this way. Following that process, a femtosecond laser is used to etch away part of the gold membrane on the ceramic ferrule end face to form two opposite electrodes. The graphene and Au have the same order of magnitude resistivity (about 10^{-6} $\Omega\cdot$ cm), and the resistance of graphene/Au composite membrane is measured to be about 20 Ω. In the final step, the optical fiber is cut flat and inserted from the other end of the ceramic ferrule and forms an F-P cavity with the suspended membrane. This process is accompanied by a high-precision mobile platform. Furthermore, the tail fiber was fixed with epoxy.

As shown in Fig. 2(a), the sensor prepared according to the above method is $\approx$ 1 cm in length and $\approx$ 2.5 mm in diameter, and a hollow channel with a diameter of 125 μm passes through it. Figure 2(b) shows the scanning electron microscope (SEM) image of the etched electrode on the ceramic ferrule end face and its local magnification. Figure 2(c) shows the Raman spectrum of the graphene membrane suspended on the end face of the ceramic ferrule. Two peaks occur at 1362 cm^{-1} and 1597 cm^{-1}, corresponding to G and 2D characteristic peaks of graphene, respectively. The relative height of the G and 2D peaks is characteristic of six to eight layers of graphene [23]. The thickness of the gold membrane was determined by sputtering Au onto a silicon wafer with the same sputtering time as on the ceramic ferrule end face. Figure 2(d) shows the profile of Au membrane as viewed through the 3D Atomic force microscope (AFM) and thickness of the gold membrane is estimated to be 72 nm.

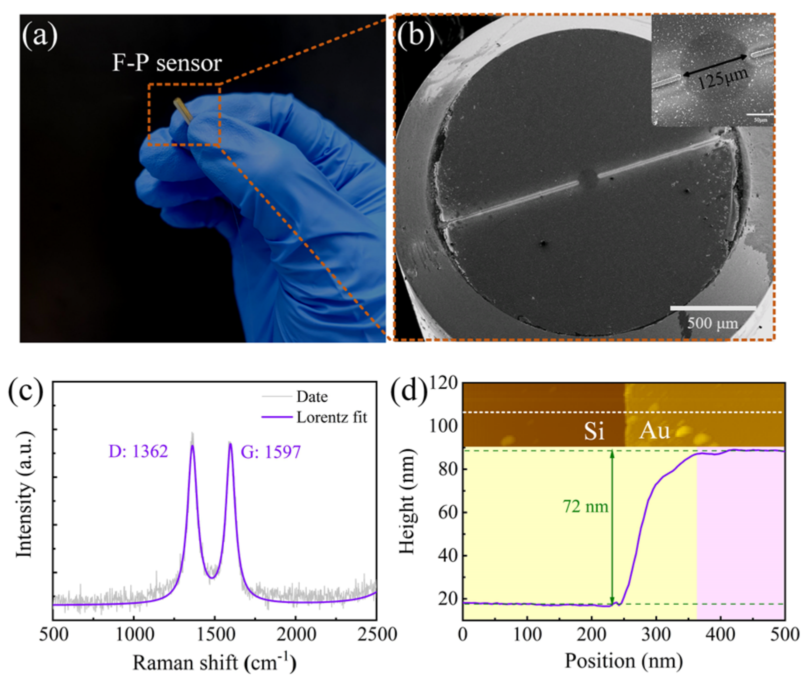

Fig. 2. (a) Photo of an F-P sensor. (b) SEM image of the ceramic ferrule end facet with the Au membrane. (c) Raman spectrum from suspended graphene measured using a 532 nm laser. (d) The height profile of Au membrane.

Due to the presence of a vertical magnetic field, Ampere force is generated when an electric current is applied to the graphene/Au film. This force stretches and deflects the membrane, resulting in change in the length of the Fabry-Perot cavity (ΔL), result in wavelength shifts ($\Delta\lambda$) in reflection spectra. The relationship between the ΔL and $\Delta\lambda$ can be expressed as [24]

$$\Delta\lambda/\lambda = \Delta L/L \tag{1}$$

where λ is the wavelength of the traced interference valley and L is the length of the cavity. As a result, the magnetic field strength can be determined by directly measuring the wavelength shift in the interference dip in the spectrum. When the Ampere force acts on the top of the membrane to shorten the cavity length, the resonant wavelength blue shifts. Conversely, when the direction of the magnetic field changes, the direction of the Ampere force acting on the membrane will also change accordingly, resulting in a red-shift of the resonant wavelength. Therefore, the magnetic field direction can be identified by detecting the resonant wavelength shift direction of the reflected spectrum of the sensor.

3. Experimental results and discussions

Figure 3 shows a typical reflection spectrum of the FPI in the range of 1530 to 1555 nm, measured with a 3 dB coupler, a broadband source (BBS), and an optical spectrum analyzer (OSA). The free spectral range (FSR) of the sensor is ~7.4 nm, corresponding to the distance between the adjacent resonance peak, as shown in Fig. 3. The length of the F-P cavity was calculated to be 161.5 µm using the formula $L = \lambda_1\lambda_2/2n_{air}(\lambda_1\text{-}\lambda_2)$, where n_{air} is the refractive index of air in the cavity. The extinction ratio (ER) was ~ 6.8 dB, and was attributed to the greater reflectivity of the gold layer compared with that of the fiber end face [25].

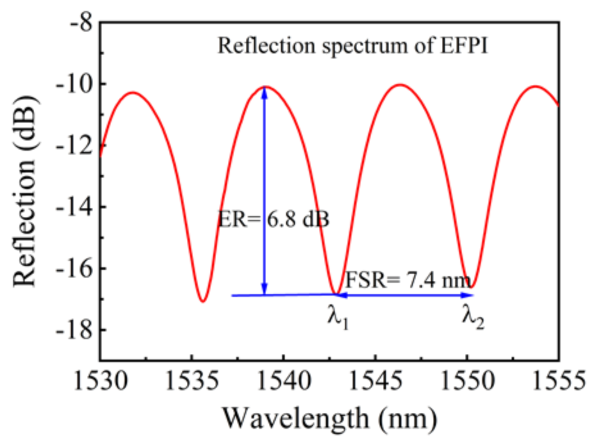

Fig. 3. A typical reflection spectrum obtained from the FPI is made with a graphene/Au membrane.

The experimental setup illustrated in Fig. 4(a) is employed to detect the magnetic field. The BBS is used to input a light with a wavelength range from 1250 to1650 nm to the magnetic sensor. And the OSA is used to record the reflection spectra of the sensor during the experiment in real-time. The magnetic field generator consists of two electromagnets, as shown in Fig. 4(a). The magnetic field strength can be adjusted by changing the driving power supply and is calibrated in real time by the Gaussian meter. In the measurement, the sensor is placed in the center of the two electromagnets and as close as possible to the calibration probe of the gauss meter. A constant current of 70 mA generated by a power source is coupled to the sensor membrane through two copper foils and is perpendicular to the direction of the magnetic field.

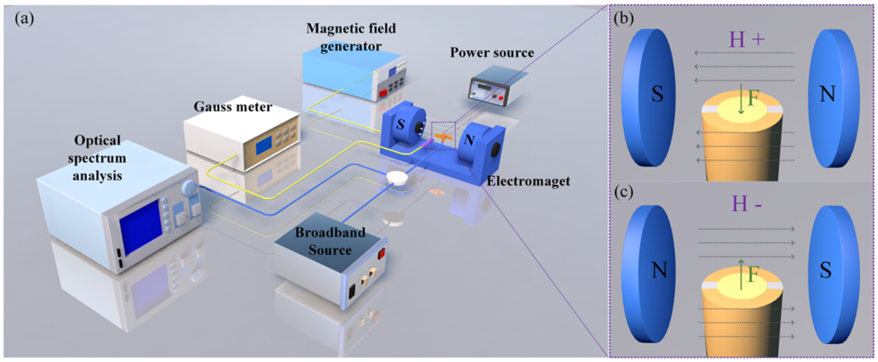

Fig. 4. (a) Schematic of the experimental setup for magnetic field measurement. Schematic diagram of the direction of Ampere force produced by graphene/Au membrane under positive (b) and negative (c) magnetic fields.

Figure 5(a) shows the reflection spectra of the sensor under the magnetic field intensity change from 0 mT to 180 mT, with the change step of 30 mT. The Ampere force perpendicular to the membrane plane downward shorten the F-P cavity length with the magnetic field increases, resulting in a blue shift in resonant wavelength. Figure 5(b) shows that there is a good linear relationship between the magnetic field intensity and the drift of resonance wavelength. The slope of the linear fitting gives a magnetic field sensitivity of ~5.71 pm/mT with a correlation coefficient (R^2) of ~0.9986. When the magnetic field intensity changes from 0 mT to -180 mT, the evolutions of reflection spectra with different magnetic intensities are shown in Fig. 5(c). The resonant wavelength of the sensor exhibits redshift with magnetic field intensity increase, which is due to the Ampere force perpendicular to the membrane plane outward, resulting in a longer F-P cavity length. Figure 5(d) shows that there is a good linear relationship between the magnetic field intensity and the drift of resonance wavelength. The slope of linear fitting between magnetic field intensity and spectral drift is ~ 8.07 pm/mT with the correlation coefficient (R^2) of ~0.9983. The sensor detection limit can be calculated as $\delta\lambda/S$, where $\delta\lambda$ is the wavelength resolution of OSA, S is sensitivity of the sensor. Considering the resolution is 0.02 nm of the OSA, the detection limit of the sensor is calculated to 2.48 mT. Since the direction of the ampere force can be adjusted by the direction of the current, the maximum sensitivity obtained here is 8.07 pm/mT.

Considering that the Young's modulus (~1 Tpa) of graphene is more than 12.8 times that of gold membrane (78 Gpa), while the thickness of graphene membrane is only 3% of that of composite membrane. Therefore, the influence of graphene deformation on the composite membrane ignored here. Assuming that the membrane is flat enough, the thickness is uniform, and the current is uniformly distributed in the membrane, the ampere force applied on the membrane through the magnetic field is also uniform. According to the elasticity of the membrane, when the deformation of a uniform flat membrane under the applied pressure is less than 30% of its thickness, the relationship between the deformation ΔL at the center of its circle and the applied pressure P can be expressed by [26]

$$\Delta L = \frac{3(1 - v^2)Pr^4}{16Eh^3} \tag{2}$$

where v and E are Poisson's ratio and Young's modulus of the Au membrane, and r and h are the radius and the thickness of the Au membrane, respectively. When electric current flows through a magnetic field perpendicular to it, the magnitude of Ampere force generated in the membrane

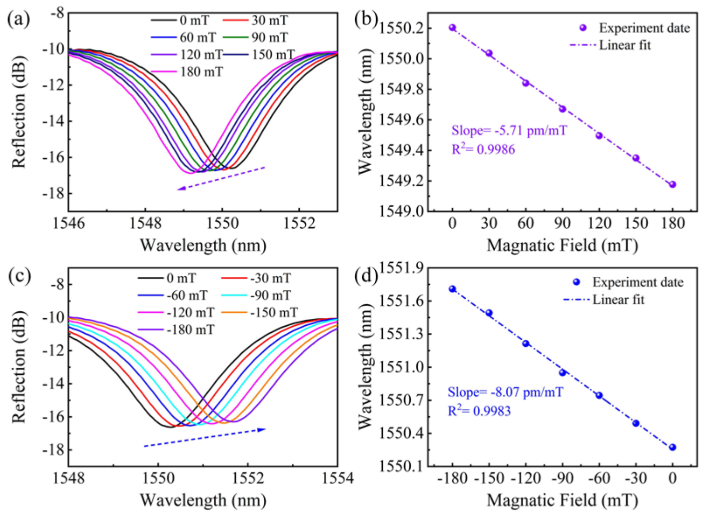

Fig. 5. Reflection spectra of the sensor at (a) 0 to 180 mT and (c) 0 to -180 mT of magnetic field intensity at 70 mA electrical current.

can be expressed by

$$F_H = I \cdot H \cdot L_H \tag{3}$$

where F_H is the Ampere force, H is the intensity of the magnetic field, I is the electrical current and L_H is the diameter of membrane. Here, the ampere force is the pressure that causes the deformation of the membrane. Substituting Eq. (3) into Eq. (2), the deformation ΔL of the membrane caused by ampere force can be determined by

$$\Delta L = \frac{3(1 - \nu^2)HIr^5}{8Eh^3} \tag{4}$$

According to Eq.1 and Eq.4, when I and r are constant, the wavelength shifts of reflection spectrum is proportional to H, which is consistent with our experimental results. It can be noted that the magnetic field sensitivity in the positive direction is smaller than that in the negative direction. As can be seen from Fig. 2(b), the diameter of the ceramic ferrule is only 125 µm, which is much smaller than the diameter of the membrane, resulting in different effective diameters for inward and outward deformation of the membrane, which leads to the difference in sensitivity between the positive and negative magnetic fields in the sensor.

The response of the magnetic field sensors is related to the magnetic field intensity H and electrical current I. To characterize the sensor's response to the electrical current, the value of the current is changed from 70 mA to 100 mA with a step size of 5 mA, while the magnetic field intensity is set at 90 mT. The reflection spectra evolutions of the sensor at different electrical current are presented in Fig. 6(a). As the electrical current increases, the resonant dip wavelength shifts to smaller wavelength. The linear fitting of the applied electrical current and dip wavelength is shown in Fig. 6(b), and the slope of the linear fitting gives an electrical current sensitivity of ~50.4 pm/mA. Therefore, when the magnetic field intensity is constant, the membrane will produce more deformation with the increase of the applied electrical current. It can be inferred that the magnetic field sensitivity of the sensor can be adjusted by changing the current.

Optics EXPRESS

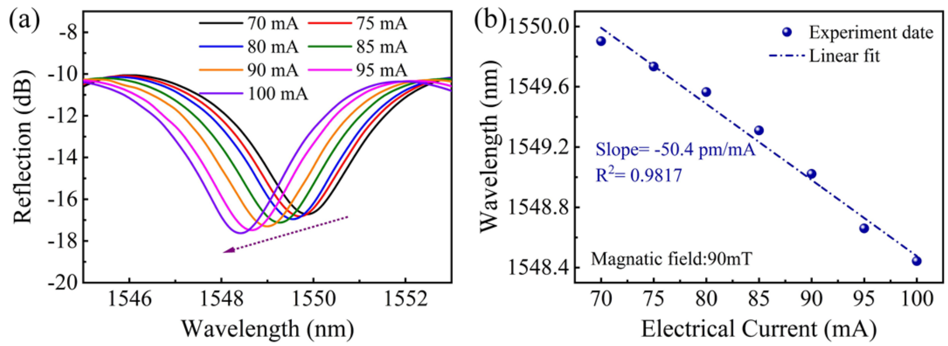

Fig. 6. (a) Reflection spectra evolution for the proposed sensor as the electrical current increased from 70~100 mA. (b) The relationship between electrical current and resonant dip wavelength.

As shown in Eq. (3), when the membrane parameters are fixed, the deformation ΔL of the membrane is proportional to the product of the magnetic field H and the electrical current I. As shown in Fig. 7, we study the relationship between the resonant dip wavelength and $I{\cdot}H$ by recalculating the data in Fig. 5(b). The result shows that the resonant dip wavelength is linear with the product value ($I{\cdot}H$), and the corresponding sensitivity is ~81.58 pm/A·mT. Here, while keeping the magnetic field constant, the Ampere force increases with the increase of the current, resulting in a shift in the resonance wavelength. In other words, applying a larger current can improve the sensitivity of the magnetic field sensor.

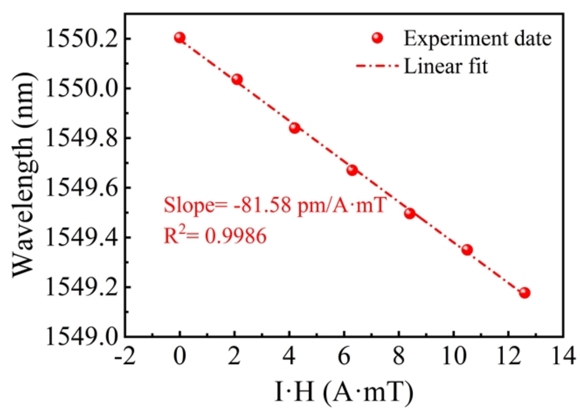

Fig. 7. Relationship between the resonant dip wavelength and I · H.

Table 1 shows the sensing performance of the fiber optic magnetic field sensor based on ampere force previously reported. These fiber optic sensors require the use of metal wires or plates to transmit ampere force to fiber optic devices for magnetic field sensing. This measurement method is indirect and increases the size of the device. The fiber optic magnetic field sensor proposed in this article is based on direct measurement and has a simple structure, wider measurement range, and the ability to distinguish the direction of the magnetic field.

Table 1. Comparison of Magnetic Field Sensors with Different Sensing Performance

Structure	Sensitivity	Range	Measurement method	Direction of discriminant
PCF with Al wire [17]	32.4 pm/mT	0~75 mT	Indirect	NO
DBR fiber laser with Cu plate [2]	258.92 kHz/mT	0~1.1 mT	Indirect	NO
Microfiber coupler with Al wire [27]	51.3 pm/mT	0~10 mT	Indirect	NO
HLPFG with Al wire [16]	456.5 pm/mT	-15~15 mT	Indirect	Yes
Fiber laser with Cu wire [18]	35.21 kHz/kGs	-4~4 kGs	Indirect	Yes
Our work	**8.07 pm/mT**	**-180~180 mT**	**Direct**	**Yes**

4. Conclusion

In conclusion, we demonstrate a Fabry-Perot interferometer based on fiber end face and graphene/Au membrane, which can achieve the measurement of magnetic field strength and direction discrimination. Due to the magnetic effect of the current, the current converts the magnetic field into an ampere force acting on the graphene/Au membrane and changes its shape. At the electrical current of 70 mA, the sensor exhibits 5.71 pm/mT positive magnetic field sensitivity and 8.07 pm/mT negative magnetic field sensitivity in the magnetic field intensity range of -180~180 mT. The sensitivity of the sensor can be optimized by changing the coupling current. The proposed sensor has the advantages of compact structure, easy to carry, cost-effective, easy to manufacture, and no magnetic saturation and hysteresis phenomenon, etc. Overall, the proposed sensor is believed to have a bright application prospect in the weak magnetic field.

Funding. Shenzhen Science and Technology Program (JCYJ20210324120403009, RCBS20200714114922296); Basic and Applied Basic Research Foundation of Guangdong Province (2021A1515011834); National Natural Science Foundation of China (62175165).

Disclosures. The authors declare no conflicts of interest.

Data availability. The datasets are available from the corresponding author on reasonable request

References

1. J. Lenz and A. S. Edelstein, "Magnetic sensors and their applications," IEEE Sensors J. **6**(3), 631–649 (2006).
2. L. Giouroudi and E. Hristoforou, "Perspective: magnetoresistive sensors for biomedicine," J. Appl. Phys. **124**(3), 030902 (2018).
3. R. Hiergeist, H. KetzlHarke Harcken, J. Ludke, M. Albrecht, T. Brand, and A. Fischer, "A novel test ground for the equipment qualification of magnetic gradient sensors used for unexploded bomb detection," J. Appl. Geophys. **112**, 242–248 (2015).
4. L. H. Cheng, J. L. Han, Z. Z. Guo, L. Jin, and B. O. Guan, "Faraday-rotation-based miniature magnetic field sensor using polarimetric heterodyning fiber grating laser," Opt. Lett. **38**(5), 688–690 (2013).
5. L. Sun, S. Jiang, and J. R. Marciante, "All-fiber optical magnetic-field sensor based on Faraday rotation in highly terbium-doped fiber," Opt. Express **18**(6), 5407–5412 (2010).
6. J. D. Lopez, A. Dante, C. C. Carvalho, R. Allil, and M. M. Werneck, "Simulation and experimental study of FBG-based magnetic field sensors with Terfenol-D composites in different geometric shapes," Measurement **172**, 108893 (2021).
7. J. Peng, S. Zhang, S. H. Jia, X. L. Kang, H. Q. Yu, S. M. Yang, S. Wang, and Y. W. Yang, "A highly sensitive magnetic field sensor based on FBG and magnetostrictive composite with oriented magnetic domains," Measurement **189**, 110667 (2022).
8. S. Yao, Y. Zhang, and B. O. Guan, "Magnetic field sensor based on the Ampere's force using dual-polarization DBR fiber laser," Opt. Rev. **22**(4), 588–592 (2015).
9. F. Zhang, B. Li, X. Y. Chen, Y. H. Gao, X. Yan, X. N. Zhang, F. Wang, T. Suzuki, Y. Ohishi, and T. L. Cheng, "A Magnetic Field Sensor Based on Birefringence Effect in Asymmetric Four-Hole Fiber," J. Lightwave Technol. **40**(8), 2594–2600 (2022).
10. J. Noda, T. Hosaka, Y. Sasaki, and R. Ulrich, "Dispersion of verdet constant in stress-birefringent silica fiber," Electron. Lett. **20**(22), 906–908 (1984).
11. D. W. Jing, L. Sun, J. Y. Jin, J. M. Thangamuthu, and J. W. Tang, "Magneto-optical transmission in magnetic nanoparticle suspensions for different optical applications: a review," J. Phys. D: Appl. Phys. **54**(1), 013001 (2021).

Optics EXPRESS

12. Z. P. Jiang, J. L. Dong, S. Q. Hu, Y. X. Zhang, Y. F. Chen, Y. H. Luo, W. G. Zhu, W. T. Qiu, H. H. Lu, H. Y. Guan, Y. C. Zhong, J. H. Yu, J. Zhang, and Z. Chen, "High-sensitivity vector magnetic field sensor based on side-polished fiber plasmon and ferrofluid," Opt. Lett. **43**(19), 4743–4746 (2018).
13. Z. H. Shao, X. G. Qiao, Q. Z. Rong, and A. Sun, "Fiber-optic magnetic field sensor using a phase-shifted fiber Bragg grating assisted by a TbDyFe bar," Sens. Actuators, A **261**, 49–55 (2017).
14. W. F. Brown, "Theory of the approach to magnetic saturation," Phys. Rev. **58**(8), 736–743 (1940).
15. E. C. Stoner and E. P. Wohlfarth, "A mechanism of magnetic hysteresis in heterogeneous alloys," Phil. Trans. R. Soc. Lond. A **240**(826), 599–642 (1948).
16. Y. Y. Zhao, S. Liu, C. Xiong, Y. Wang, Z. Y. Li, Z. Y. Sun, J. Q. Li, and Y. P. Wang, "Magnetic field sensor based on helical long-period fiber grating with a three-core optical fiber," Opt. Express **29**(13), 20649–20656 (2021).
17. S. J. Qiu, Q. Liu, F. Xu, and Y. Q. Lu, "Ampere force based photonic crystal fiber magnetic field sensor," Sens. Actuators, A **210**, 95–98 (2014).
18. W. R. Cheng, T. M. Luo, L. H. Cheng, H. Liang, and B. O. Guan, "Miniature fiber-optic magnetic field sensor based on ampere force and fiber laser," Photonic Sens **10**(4), 291–297 (2020).
19. S. Liu, Y. P. Chen, H. L. Lai, M. Q. Zou, H. Xiao, P. J. Chen, B. Du, X. Z. Xiao, J. He, and Y. P. Wang, "Room-temperature fiber tip nanoscale optomechanical bolometer," ACS Photonics **9**(5), 1586–1593 (2022).
20. F. F. Yu, Q. W. Liu, X. Gan, M. X. Hu, T. Y. Zhang, C. Li, F. Y. Kang, M. Terrones, and R. T. Lv, "Ultrasensitive pressure detection of few-layer MoS_2," Adv. Mater. **29**(4), 1603266 (2017).
21. J. Ma, Y. L. Zhou, X. Bai, K. Chen, and B. O. Guan, "High-sensitivity and fast-response fiber-tip Fabry-Perot hydrogen sensor with suspended palladium-decorated graphene," Nanoscale **11**(34), 15821–15827 (2019).
22. J. Ma, W. Jin, H. T. Xuan, C. Wang, and H. Hoi Lut, "Fiber-optic ferrule-top nanomechanical resonator with multilayer graphene film," Opt. Lett. **39**(16), 4769–4772 (2014).
23. A. C. Crowther, A. Ghassaei, N. Jung, and L. E. Brus, "Strong charge-transfer doping of 1 to 10 layer graphene by NO_2," ACS Nano **6**(2), 1865–1875 (2012).
24. J. Ma, J. Ju, L. Jin, and W. Jin, "A compact fiber-tip micro-cavity sensor for high-pressure measurement," IEEE Photonics Technol. Lett. **23**(21), 1561–1563 (2011).
25. S. Liu, P. J. Chen, J. X. Luo, Y. P. Chen, B. N. Liu, H. Xiao, W. Q. Yan, W. Ding, Z. Y. Bai, J. He, and Y. P. Wang, "Nano-optomechanical resonators based graphene/Au membrane for current sensing," J. Lightwave Technol. **40**(21), 7200–7207 (2022).
26. M. D. Giovanni, *Flat and Corrugated Diaphragm Design Handbook*(CRC, 1982).
27. S. C. Yan, Y. Chen, C. Li, F. Xu, and Y. Q. Lu, "Differential twin receiving fiber-optic magnetic field and electric current sensor utilizing a microfiber coupler," Opt. Express **23**(7), 9407–9414 (2015).